Int. J. Rock Mech. Min. Sci. & Geomech. Abstr. Vol. 12, pp. 335–340. Pergamon Press 1975. Printed in Great Britain

The Effect of Humidity on the Compliances of Coal Mine Shales

EDWARD M. VAN EECKHOUT*
SYD S. PENG†

The transversely isotropic compliance characteristic of three United States coal mine shales is investigated. Tests on specimens stabilized at 0, 48 and 100 per cent relative humidity show not only a change of strength with humidity but a change in observed compliances as well. Young's moduli values obtained for 'dry' specimens were on the order of two or three times that of the 'wet' specimens. This has important implications for any computer modeling program using these types of shale.

INTRODUCTION

As structural analyses of mining operations become more and more sophisticated by computer modeling, good estimates of the mechanical behavior of various rock types are necessary. Unfortunately, this information appears to be quite deficient for some rocks in the literature. This deficiency is particularly evident for coal mine shales, the most common rock type immediately overlying coal. Since roof falls account for greater than 50 per cent of coal mine fatalities, a more detailed understanding of the mechanical behavior of coal mine shales is certainly warranted, especially that exhibited under the varying humidity conditions experienced in coal mines. These humidity fluctuations are evidenced by moisture condensation on the rock during the summer and drying-out of the rock during the winter due to temperature differentials. Hence the purpose of this paper is to investigate coal mine shale compliances and the effect of humidity on them.

The bedded nature of shales generally suggests that they may exhibit rotational symmetry in their mechanical properties, and they are consequently usually modeled as transversely isotropic (characterized by five independent elastic constants) in their elastic behavior. Apparently, the only published data on the compliances of shale to any degree of detail is that given by Chenevert and Gatlin [3]. It is reproduced in Table 1 below, using the '3' direction as perpendicular to bedding (see Appendix A for a review of the form of the transversely isotropic compliance matrix and conventions used in this paper).

No independent shear moduli (S_{44}) values seem to have been determined for shales. Other published data on shales (e.g. [2]) do not give direction values.

The effect of moisture on rock compliances has been somewhat investigated, but not with reference to directional properties. Shale-like rocks appear to have the greatest change of compliance with moisture, as observed from the Young's moduli tabulated from various sources in Table 2.

Hence it appears that few details are known about the effect of moisture on coal mine shale compliances and is a subject worthy of further study.

MATERIAL DESCRIPTION

Samples from three Appalachian coal mines were selected for this study:

(1) a massive-appearing roof shale from the Beatrice Mine of Island Creek Coal Co., Keen Mountain, VA;

(2) a well laminated roof shale from the Matthew Mine of Consolidation Coal Co., Middlesboro, KY; and

(3) a blocky floor shale from the Armco Mine of Armco Steel Corp., Mountcoal, West VA.

*Continental Oil Co., P.O. Box 1267, Ponca City, OK 74601, U.S.A.

†College on Mineral and Energy Resources, West Virginia University, Morgantown, WV 26506, U.S.A.

TABLE 1. ELASTIC DATA FOR SHALES

Rock	Compliances* (10^{-6} $(MN/m^2)^{-1}$)					Source
	S_{11}	S_{33}	S_{44}	S_{12}	S_{13}	
Green River Shale	28.4	33.7	–	4.3	6.1 6.4	Chenevert and Gatlin (1965)
Permian Shale	30.2	41.4	–	5.4	6.3 5.4	Chenevert and Gatlin (1965)

* 1 MN/m^2 = 145 psi = 10 bars

TABLE 2. COMPARISON OF WET VERSUS DRY YOUNG'S MODULI FOR CERTAIN ROCKS

Rock Type	Young's Modulus Wet/Dry	Source
dolerite	.97	Wiid (1970)
quartzitic sandstone	.75	
sandstone	.84	
sandstone	.7	Nishihara (1957)
silty shale	.43	Hermann et al (1937)
arenaceous sh	.7	

These samples were collected from actual strata failures by Dr. T. C. Shelton of the Virginia Polytechnic Institute as part of a U.S. Bureau of Mines shale procurement program. The samples were enclosed in plastic bags, placed in 55-gal drums, and shipped to the Twin Cities Mining Research Center, U.S. Bureau of Mines, Twin Cities, MN.

Detailed descriptions of the geologic properties of each rock type sampled are given elsewhere [12]. All three had predominantly illite, quartz, and chlorite as the major minerals (some kaolinite was found in the Matthews shale); the vacuum dried porosity was between 1–3 per cent; and the permeabilities observed were low to nil over short period of time (a few hours). In addition, preferred mineral orientation by X-ray diffraction on disks [1,6] and acoustic velocity stereonets of spheres [9] indicated that indeed there was preferred mineral and acoustic velocity orientation and that the largest divergence of values occurred between poles in the bedding plane and perpendicular to it. A typical acoustic velocity stereonet of Beatrice shale is shown in Fig. 1. It is assumed for the purposes of this paper that the material is transversely isotropic, even though there were indications that the Matthews shale in particular might, in fact, be nearer to orthotropic. There are few applications where this distinction would be of great concern.

SAMPLE PREPARATION AND HUMIDITY CONTROL

The bedding configuration of a sample block was determined and prisms were cut in the direction desired using wire and circular saws. The specimens were kept small in size (on the order of 2·5 cm dia by 5 cm long) to facilitate moisture conditioning. The specimen surfaces were ground flat and parallel to within $\pm 0{\cdot}0025$ cm longitudinally and $\pm 0{\cdot}01$ cm laterally. Slabbing was especially severe in Matthews, which was the reason prisms were made originally (it was thought that the wire and circular saws would minimize slabbing as opposed to coring, but it generally did not make a great deal of difference in number of successful attempts). A 50 per cent success rate in Matthews and higher rates in the other shale types were obtained in sample preparation. Water was used in all processes, but because of the short exposure time, it should not have appreciably affected the samples (some samples were made without water cooling, but this only overheated the bits and yielded no increase in success rate).

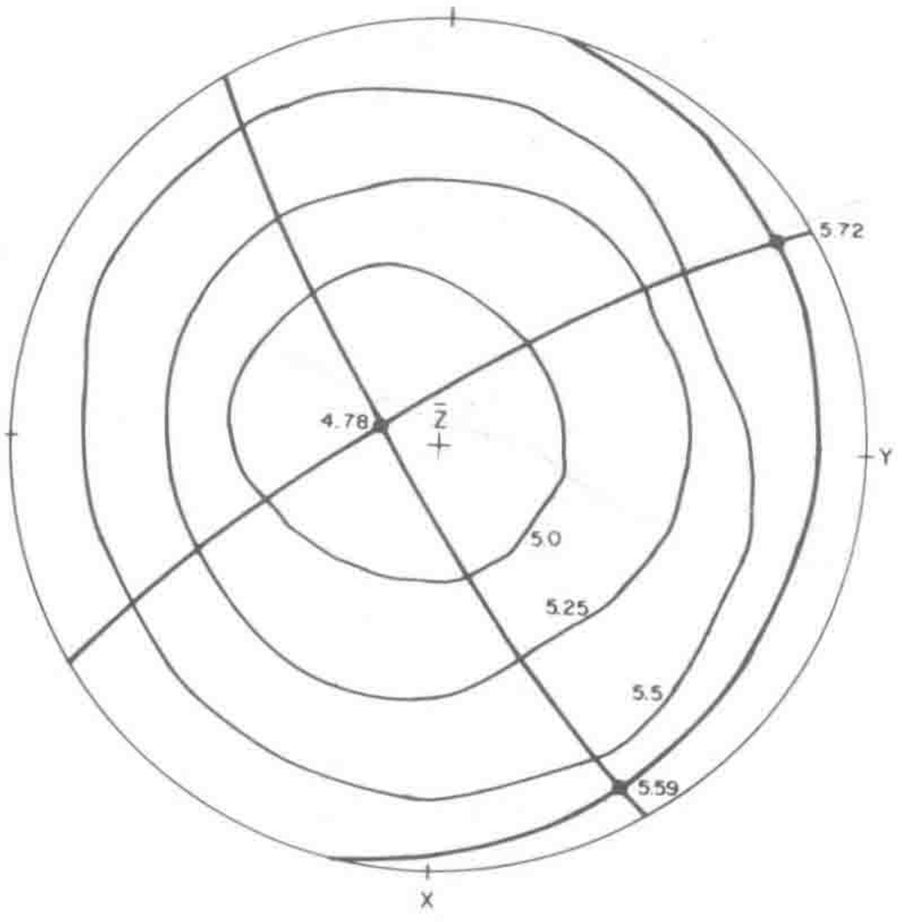

Fig. 1. Beatrice pulse velocity stereonet (km/sec).

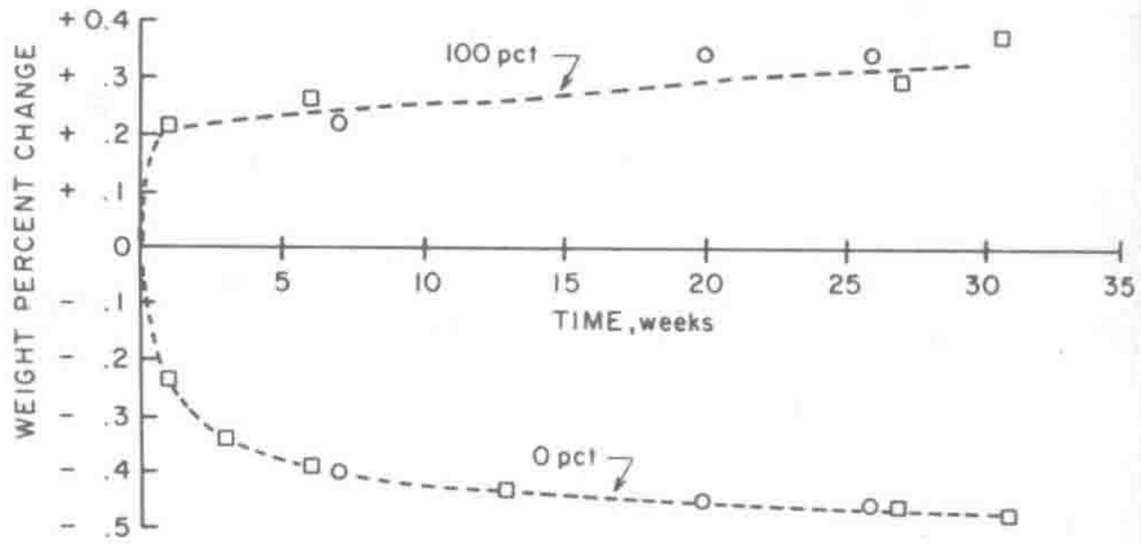

Fig. 2. Weight change with time for Beatrice shale.

Before testing, samples were placed in desiccators stabilized at approximately 0, 48 and 100 per cent relative humidity. These humidities were attained by using a drying desiccant and saturated salt solutions [11]. Since these rocks were quite nonporous and impermeable, time for moisture stabilization (defined as no appreciable weight change in a week or two) from one humidity to another was expected to be quite long, which in fact was found to be the case. Samples to be monitored for water absorption were first placed in a desiccator maintained at 48 per cent relative humidity as a base (since the samples had been exposed to wet–dry cycling already, there was no way of determining the original moisture condition). This stabilization generally required about one month. The samples were then transferred to the other desiccators and taken out for periodic weighings. The samples were disturbed as little as possible in order to maintain the humidity desired, and the weighings were done as quickly as possible (about 1–5 min), after which the samples were returned to the desiccators.

Figure 2 presents the moisture contents versus time history for intact Beatrice shale prisms when taken from 48 per cent humidity to 0 and 100 per cent. There is more scatter in the readings at 100 per cent humidity, probably due to water collection on the surface of the specimen with subsequent evaporation before and during weighing. The curves indicate that the moisture had not completely stabilized even after 30 weeks, but given the finite time involved in this study, it was decided to stabilize specimens at least 6 weeks before testing and preferably longer. Stabilization times for the Matthews and Armco shales were similar.

EXPERIMENTAL TECHNIQUE

The transversely isotropic compliance matrix was determined by testing the rock in the three independent orientations shown in Fig. 3.

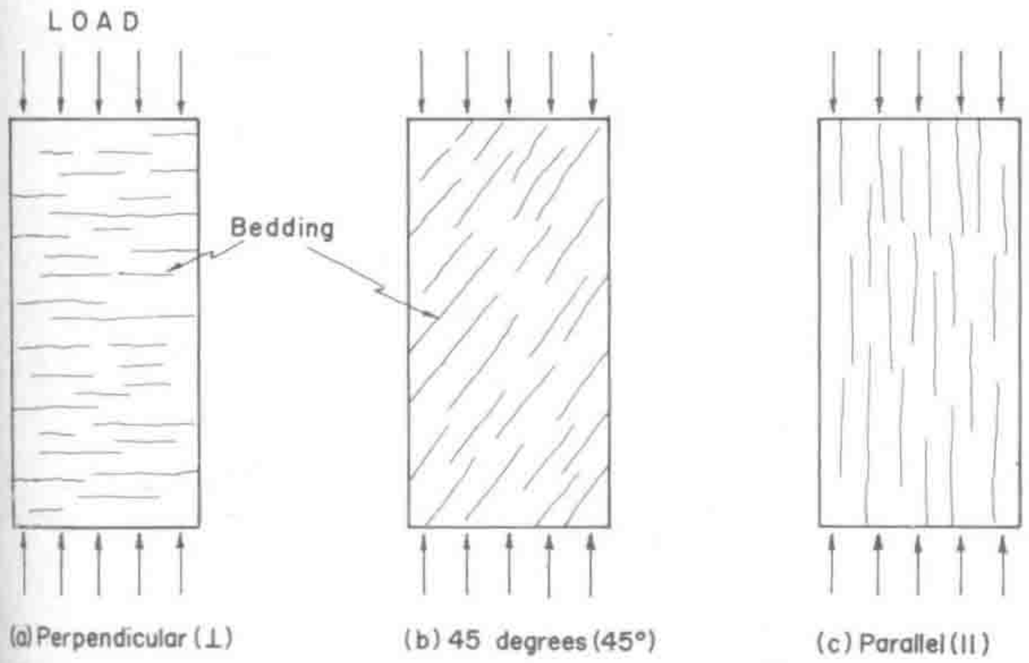

Fig. 3. Test configurations used to determine compliance values, with load vs bedding orientation noted.

Longitudinal and lateral deformations were monitored; the average engineering elastic 'constants' as defined in Appendix A were computed and used to compute S_{11}, S_{12}, S_{33}, and S_{13}.

However, the computation of S_{44}, the independent shear compliance, was somewhat more complicated. The particular test orientation used for that computation was that shown in Fig. 3(b). Since load was not applied along a major compliance axis, a platen–rock shear force τ would be expected to develop in addition to the normal stress σ which should be related to the observed strains in the following manner:

$$\epsilon_{\text{longitudinal}} = S'_{11}\sigma + S'_{16}\tau$$
$$\epsilon_{\text{lateral}} = S'_{13}\sigma + S'_{26}\tau \quad (1)$$

where the primed compliances are the transformed values.

Substituting the relationship between transformed and principal compliances at direction cosines m and l [4] and dividing by the normal stress,

$$\frac{\epsilon_{\text{long.}}}{\sigma} = [m^4 S_{11} + 2m^2 l^2 S_{13} + l^4 S_{33} + m^2 l^2 S_{44}] + [-2m^3 l S_{11} + 2(m^3 l - ml^3)S_{13} + 2ml^3 S_{33} + (m^3 l - ml^3)S_{44}]\frac{\tau}{\sigma} = \frac{1}{E'} \quad (2)$$

$$\frac{\epsilon_{\text{lat.}}}{\sigma} = [m^2 l^2 S_{11} + (m^4 + l^4)S_{13} + m^2 l^2 S_{33} - m^2 l^2 S_{44}] + [-2ml^3 S_{11} + 2(ml^3 - m^3 l)S_{13} + 2m^3 l S_{33} + (ml^3 - m^3 l)S_{44}]\frac{\tau}{\sigma} = \frac{\nu'}{E'}. \quad (3)$$

These equations are greatly simplified for the case indicated in Fig. 3(b) since the 45-degree load vs bedding orientation was used. Using the direction cosine for 45 degrees and subtracting (3) from (2), the relation reduces to:

$$\frac{\epsilon_{\text{long.}} - \epsilon_{\text{lat.}}}{\sigma} = 0{\cdot}5\, S_{44} \quad (4)$$

or,

$$S_{44} = 2\left(\frac{1 + \nu_{45^\circ}}{E_{45^\circ}}\right).$$

Fig. 4. 2000 kN Capacity testing equipment.

Hence S_{44} is a simple calculation for this particular orientation, but if orientations other than 45 degrees are used, it becomes much more complex as seen by equations (2) and (3).

To collect the required data, a 2000 kN MTS hydraulic servo-controlled testing machine was used for applying loads to the specimens. This unit is shown in Fig. 4. The loads were monitored with load cells placed immediately above the machine platens.

Longitudinal deformations were monitored with the LVDT's (linear variable differential transformers) shown in Fig. 4, while lateral deformations were monitored with DCDT's (direct current differential transformers) as shown in Fig. 5. These devices were chosen rather than strain gauges because of their simplicity in setting up and their ability to monitor after detectable sample cracking.

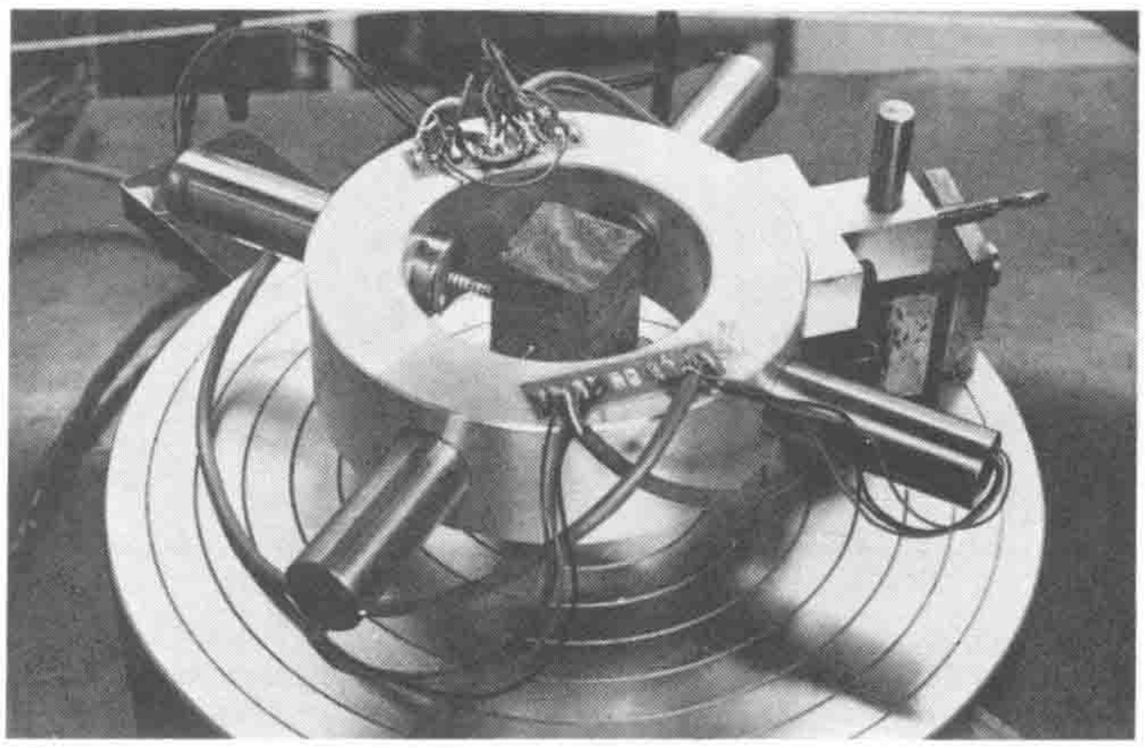

Fig. 5. DCDT lateral monitors.

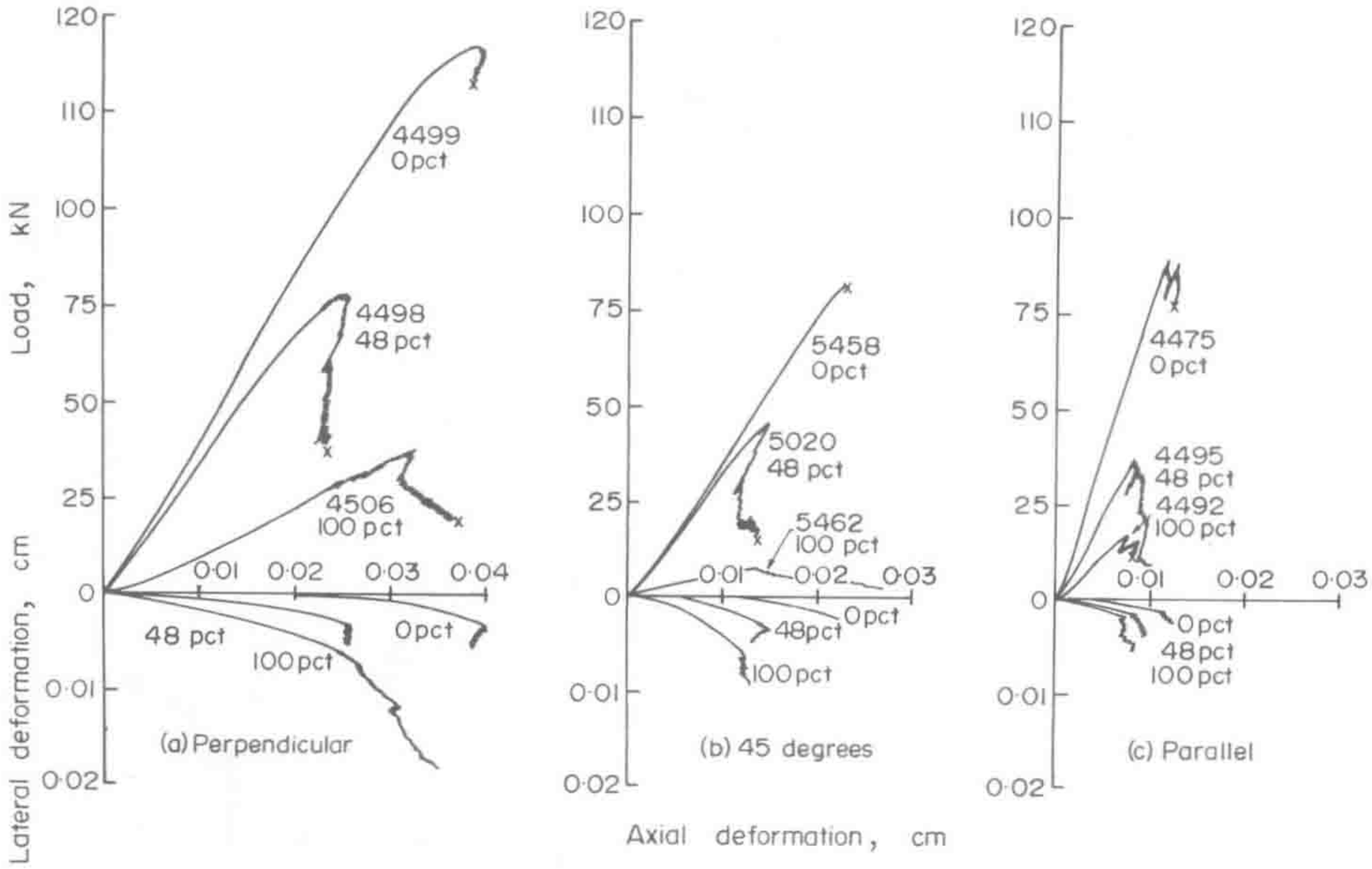

Fig. 6. Typical Beatrice load–deformation curves, with load vs bedding orientation noted.

Two systems were used for data output: a Vidar data punch machine and two Hewlett–Packard x–y–y recorders. These systems recorded the raw data, to which the proper calibration factors and platen deformation corrections were applied.

All testing was designed so that peak load was reached in approximately 10 min. This allowed enough time for "quasi-static" tests while minimizing moisture changes during testing. Specimens were placed between steel platens of the same cross section for testing. No spherical seats were used, since they tended to rotate once fracturing began, hence decreasing test 'control' after the peak load was reached. A constant specimen lateral deformation rate was programmed, again allowing for greater 'control' after peak load was reached.

TABLE 3. BEATRICE SHALE ELASTIC CONSTANTS OBSERVED

Humidity	Orientation of load to bedding	$E(10^3$ MN/m$^2)$	$\nu_{\parallel}$	ν_{45°	$\nu_{\perp}$
0 pct	//	56.6 (9.2) N=4	.164 (.024) N=4	-	.574 (.507) N=4
	45°	38.0 (6.8) N=4	.142 (.011) N=4	.264 (.035) N=4	-
	⊥	31.6 (3.5) N=6	.112 (.040) N=12	-	-
48 pct	//	40.8 (2.7) N=4	.047 (.006) N=4	-	.404 (.090) N=4
	45°	31.3 (3.0) N=4	.174 (.017) N=4	.340 (.023) N=4	-
	⊥	29.9 (1.4) N=4	.195 (.034) N=8	-	-
100 pct	//	21.8 (6.4) N=6	.016 (.087) N=6	-	1.89 (1.9) N=6
	45°	9.6 (2.3) N=2	.09 (.13) N=2	1.3 (1.3) N=2	-
	⊥	12.8 (2.1) N=4	.416 (.079) N=8	-	-

RESULTS

Typical load–deformation curves for the Beatrice shale are given in Fig. 6. Those for Matthews and Armco were similar in nature, although not all three humidities were represented in the 45-degree orientation. Note how the curves show decreasing elasticity and peak load with increasing humidity. The

TABLE 4. MATTHEWS SHALE ELASTIC CONSTANTS OBSERVED

Humidity	Orientation of load to bedding	$E(10^3$ MN/m$^2)$	$\nu_{\parallel}$	ν_{45°	$\nu_{\perp}$
0 pct	//	39.5 (4.5) N=4	.027 (.028) N=4	-	.136 (.023) N=4
	⊥	23.3 N=1	.121 N=2	-	-
	//	34.0 (5.2) N=6	.065 (.021) N=6	-	.330 (.145) N=6
48 pct	45°	21.4 (6.4) N=4	.040 (.044) N=4	.161 (.034) N=4	-
	⊥	23.8 (0.7) N=3	.184 (.013) N=6	-	-
100 pct	//	16.2 (2.7) N=6	.087 (.040) N=6	-	.865 (.531) N=6
	⊥	10.5 N=1	.385 N=2	-	-

TABLE 5. ARMCO SHALE ELASTIC CONSTANTS OBSERVED AVERAGE OF TWO SAMPLES

Humidity	Orientation of load to bedding	E(10^3 MN/m^2)	$\upsilon_{\parallel}$	υ_{45°	$\upsilon_{\perp}$
0 pct	//	38.0	.018	-	.082
	45°	32.0	.029	.104	-
	⊥	29.5	.152	-	-
48 pct	//	35.5	.261	-	.248
	45°	21.1	.020	.116	-
	⊥	29.0	.202	-	-
100 pct	//	34.4	.314	-	.497
	45°	16.2	.100	.264	-
	⊥	14.9	.413	-	-

cause of peak load reduction is interesting in itself, requiring further investigations than shown here, and will be the subject of another paper. The elastic 'constants' were compiled for curves such as these by averaging secant values between 5 kN and one-half peak load. The results of these computations are given in Tables 3, 4 and 5 for the three shale types. In those tables, the subscript on Poisson's ratio is the direction monitored in relation to bedding (see Appendix A), each value in parentheses is one standard deviation, and N is the number of tests for each data point. The standard deviations for the Armco results (Table 5) were not computed, since only two values were obtained for each point. As mentioned earlier, further computations can be made to convert these results to compliances, which was done for the Beatrice and Matthews shales (Table 6).

DISCUSSION AND CONCLUSION

The results in Table 6 indicate one clear trend: an increase in compliance with increased moisture (i.e. a decrease in Young's modulus E and an increase in Poisson's ratio v). The load–deformation curves presented earlier (Fig. 6) also indicate this trend. The change in compliances from 0 to 48 per cent humidity was much less marked than from 48 to 100 per cent humidity. This was especially evident for S_{33}, but there is one notable exception to this, S_{12} for the Beatrice shale. Table 3 shows very high standard deviation for $v_{\perp\parallel}$, most probably due to the premature cracking often observed when loaded parallel to bedding. It was because of this consideration that S_{13} was used in Table 6 instead of S_{31}. If an unusually large $v_{\perp\parallel}$ was noted, one would expect a small $v_{\parallel\parallel}$, since the material was no longer continuous. In addition, this was the direction in which an unexpected observation was made: that of lateral contraction initially, with expansion at higher loads (one would expect all contraction or expansion in the elastic zone). This phenomenon was noted quite early in the testing program and is discussed elsewhere [12]. Because of this premature cracking and initial contraction, it is not too surprising that this particular compliance does not agree with the others in trends observed.

This study does show that moisture affects the compliances observed (those taken directly from the load–deformation curves), and the logical reason for this is the loss of grain to grain contact area and an increase or decrease of capillary tension between grains (due to the encroachment of water in the pores).

It is quite interesting to note in Table 6 how rapidly S_{33} rises at 100 per cent humidity while the rise of S_{11} seems to be a bit more gradual. This is probably due to mineral grain orientation effects (i.e. somewhat like the difference between adding water between a deck of cards and then compressing a stack of cards perpendicular and parallel to the cards and comparing the results with a deck without water).

Practically speaking, this change of compliance with moisture could have a profound effect on a coal mine roof, for incoming air tends to condense on the mine rock as it is cooled in the summer and dry out the mine rock as it is heated in the winter. In addition, this wet–dry cyclic change is aggravated by the use of water for dust suppression at the face. If moisture is absorbed into the roof shale, the roof will tend to relax due to its lower elasticity, but this may be compensated by the tendency to swell with greater moisture content. However, if moisture is desorbed from the roof shale, the roof will tend to contract due both to increased elasticity and the natural contraction of shale as it dries

TABLE 6. COMPLIANCES OBSERVED [10^{-6}(MN/m^2)$^{-1}$]

	BEATRICE			MATTHEWS		
	0 pct	48 pct	100 pct	0 pct	48 pct	100 pct
S_{11}	18. (3.) N=4	25. (2.) N=4	46. (14.) N=6	25. (3.) N=4	29. (4.) N=6	62. (10.) N=6
S_{33}	32. (3.) N=6	33. (1.) N=4	78. (13.) N=4	43. N=1	42. (1.) N=3	95. N=1
S_{12}	- 3. (1.) N=4	- 1. (1.) N=4	- 1. (4.) N=4	-1. (1.) N=4	- 2. (1.) N=6	- 5. (2.) N=6
S_{13} [1]	- 4. (1.) N=12	- 7. (1.) N=8	- 32. (8.) N=8	-5. N=2	- 8. (1.) N=6	- 37. N=2
S_{44} [2]	67. (8.) N=4	86. (6.) N=4	468. (264.) N=2	-	108. (29.) N=4	-

[1] Theoretically, $S_{13} = S_{31}$, but from the data obtained, S_{13} appeared more reliable, and in most cases S_{31} was within any reasonable experimental error. Consequently, S_{13} was used.

[2] S_{44} was computed from the 45° tests as indicated in the text.

out. This contraction will often be great enough to break the shale in tension.

In addition, roof shale is often interrupted by foreign structures such as kettle bottoms, horsebacks, or other discontinuities, making the problems even more severe. In order to determine the exact influence of humidity changes in a particular mine, field data is needed and is the next logical step to this study.

Acknowledgement—Financial support for this work was provided by the Twin Cities Research Center of the U.S. Bureau of Mines, where the entire project was conducted. Although many from that center assisted in the experiments, particular thanks are due H. Kuhlman, D. West, and R. Rosenquist for all the assistance in gathering data and preparing samples.

Received 7 January 1975.

REFERENCES

1. Bennetts K. P. Orientation index determination of flint clay using an X-ray diffractometer technique. *S. Afr. Geol. Survey Annls* **2,** 161–168 (1963).
2. Birch F. Compressibility; elastic constants in *Handbook of Physical Constants*, (Ed. Clark), GSA Memoir Vol. 97, pp. 97–174 (1966).
3. Chenevert M. E. and Gatlin C. Mechanical anisotropies of laminated sedimentary rocks. *Soc. Petrol. Engng J.* 67–77 (March 1965).
4. Hearmon R. F. S. *An Introduction to Applied Anisotropic Elasticity*, p. 136. Oxford University Press, Oxford (1961).
5. Hermann H., Stocke K. and Udluft H. Ground pressure and plate-statics tests on the elastic properties of coal-measure rocks from upper-Silesian mines. *Beitr. angew. Geophys.* **6,** 206–240 (1937).
6. Jaeger J. C. and Cook N. G. W. *Fundamentals of Rock Mechanics*, p. 513. Methuen, London (1969).
7. Meade R. H. X-ray diffractometer method for measuring preferred orientation in clays, U.S.G.S. Prof. Paper 424–B, p. 4 (1961).
8. Nishihara M. Stress–strain relation of rocks. *Doshisha Engng Rev.* **8,** 32–54 (1957).
9. Thill R. E., Willard R. J. and Bur T. R. Correlation of longitudinal velocity variation with rock fabric. *J. Geophys. Res.* **74,** 4897–4909 (1969).
10. Wiild B. L. The influence of moisture on the pre-rupture fracturing of two rock types, in *Proc. 2nd Int. Conf. Rock Mech.* Vol. 2, pp. 239–245, Belgrade (1970).
11. Winston P. W. and Bates D. H. Saturated solutions for the control of humidity in biological research. *Ecology* **41** (1), 232–237 (1960).
12. Van Eeckhout E. M. The effect of moisture on the mechanical properties of coal mine shales. Ph.D. Dissertation, University of Minnesota (1974).

APPENDIX A

The most general expression for the linear elastic strain–stress relationship is the following:

$$\{\epsilon\} = [S]\ \{\sigma\} \tag{A-1}$$

where

ϵ = infinitesimal strain,
S = compliance, and
σ = stress

as defined in the usual manner (see e.g. [6]). For a transversely isotropic material (hexagonal symmetry), the compliance matrix is reduced to 5 independent compliances. If one chooses axes parallel

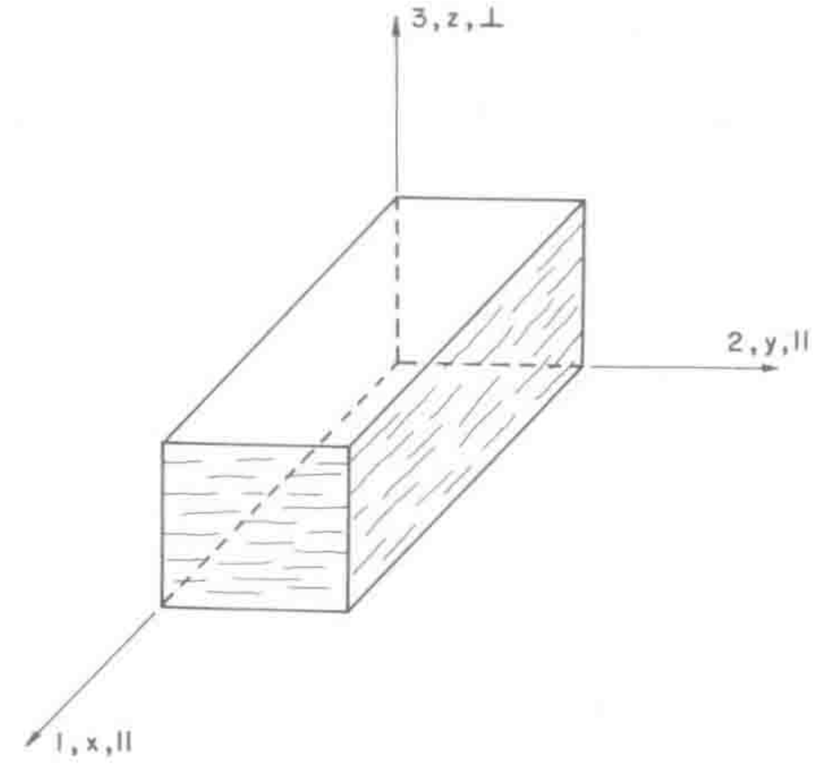

Fig. A1. Relation of bedding to x, y, z axes.

to the principal strain axes, the $[S]$ matrix would appear as follows:

$$S_{\text{tr. is.}} = \begin{bmatrix} S_{11} & S_{12} & S_{13} & 0 & 0 & 0 \\ S_{12} & S_{11} & S_{13} & 0 & 0 & 0 \\ S_{13} & S_{13} & S_{33} & 0 & 0 & 0 \\ & & & S_{44} & & \\ & & & & S_{44} & \\ & & & & & 2(S_{11}-S_{12}) \end{bmatrix} \tag{A-2}$$

using the directional notation as shown in Fig. A1.

Within this framework the compliance matrix can be expressed in terms of 'engineering elastic constants' as follows:

$$S_{\text{tr. is.}} = \begin{bmatrix} \frac{1}{E_{\parallel}} & -\frac{\nu_{\parallel\parallel}}{E_{\parallel}} & -\frac{\nu_{\parallel\perp}}{E_{\perp}} & 0 & 0 & 0 \\ -\frac{\nu_{\parallel\parallel}}{E_{\parallel}} & \frac{1}{E_{\parallel}} & -\frac{\nu_{\parallel\perp}}{E_{\perp}} & 0 & 0 & 0 \\ -\frac{\nu_{\perp\parallel}}{E_{\parallel}} & -\frac{\nu_{\perp\parallel}}{E_{\parallel}} & \frac{1}{E_{\perp}} & 0 & 0 & 0 \\ 0 & 0 & 0 & \frac{1}{G_{\parallel\perp}} & 0 & 0 \\ 0 & 0 & 0 & 0 & \frac{1}{G_{\perp\parallel}} & 0 \\ 0 & 0 & 0 & 0 & 0 & \frac{2(1+\nu_{\parallel\parallel})}{E_{\parallel}} \end{bmatrix}$$

where

$E_{\parallel}$ = Young's modulus in the x–y plane,
$E_{\perp}$ = Young's modulus perpendicular to the x–y plane,
$\nu_{\parallel\parallel}$ = Poisson's ratio in the x–y plane due to a force applied in the same plane,
$\nu_{\perp\parallel}$ = Poisson's ratio perpendicular to the x–y plane due to a force applied in the x–y plane,
$\nu_{\parallel\perp}$ = Poisson's ratio in the x–y plane due to a force applied perpendicular to it,
$G_{\perp\parallel} = G_{\parallel\perp}$ = shear constant between the x–y plane and any other plane perpendicular to it.

These definitions are perhaps clearer in reference to Fig. A2. In addition, since

$$\frac{\nu_{\parallel\perp}}{E_{\parallel}} = \frac{\nu_{\perp\parallel}}{E_{\perp}},$$

these six constants defined above reduce to five independent values, the number required for a transversely isotropic material.

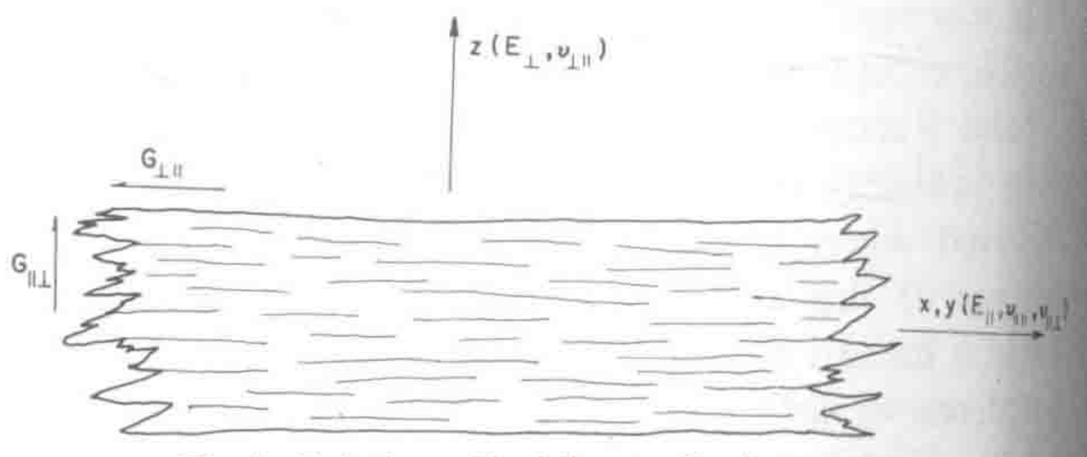

Fig. 2. Relation of bedding to elastic constants.